Delft University of Technology

Delft Center for Systems and Control

Technical report 20-008

A multi-class urban traffic model considering heterogeneous vehicle composition: An extension of the S model*

C. Portilla, J. Espinosa, and B. De Schutter

If you want to cite this report, please use the following reference instead:

C. Portilla, J. Espinosa, and B. De Schutter, "A multi-class urban traffic model considering heterogeneous vehicle composition: An extension of the S model," *Transportation Research Part C*, vol. 115, June 2020. Article 102613. doi:10.1016/j.trc.2020.102613

Delft Center for Systems and Control
Delft University of Technology
Mekelweg 2, 2628 CD Delft
The Netherlands
phone: +31-15-278.24.73 (secretary)
URL: https://www.dcsc.tudelft.nl

*This report can also be downloaded via https://pub.bartdeschutter.org/abs/20_008.html

A multi-class urban traffic model considering heterogeneous vehicle composition: an extension of the S model

C. Portilla[a], J. Espinosa[a], B. De Schutter[b]

[a] *Facultad de Minas,*
Universidad Nacional de Colombia, Medellín, Colombia.
[b] *Delft Center for Systems and Control,*
Delft University of Technology, Delft, The Netherlands

Abstract

In this paper a new multi-class urban traffic model is proposed based on the features of a single-class urban traffic model and the characteristics of a multi-class freeway traffic model. The heterogeneous traffic flow is represented using the concept of Passenger Car Equivalent (PCE) for congestion and free-flow regimes separately. The proposed multi-class urban traffic model is intended for model-based control applications. The single-class model and the proposed multi-class traffic model are compared with microscopic simulation data obtained using the SUMO (Simulation of Urban MObility) open-source simulator. The two models are calibrated through optimal parameter estimation and their performance is evaluated and compared by taking into account the error index between the models and the simulation data. Simulation results show that the multi-class model gives a significantly better fit.

Keywords: `Urban traffic network, macroscopic traffic model, Passenger Car Equivalent (PCE), heterogeneous traffic, traffic simulation.`

1. Introduction

Nowadays, modern major cities have problems resulting from their accelerated and often uncontrolled growth. One of these are traffic jams, which affect mobility and have adverse environmental, social, and economic impacts. Efficient management of the traffic network can reduce congestion and its associated consequences such as emission of polluting gases, fuel consumption, noise, accident rates, and waiting times.

In order to solve these mobility problems, it is important to implement efficient and effective online (monitoring and control) and offline (planning of new roads, government policy measures) management strategies for the urban traffic network. Usually, these strategies require an urban traffic representation, i.e., a dynamic mathematical model that describes the evolution of the traffic flows in the system. However, urban traffic is not homogeneous as there are several types of vehicles on the road: cars, sport utility vehicles (SUVs), vans, buses, trucks, and motorcycles, with their own characteristics such as engine power, weight, and size. As a result, the vehicle flow is a composition of different types of vehicles interacting with each other and their characteristics should be represented by the mathematical model. In addition, this model should have a high accuracy and, as it is used for on-line model-based applications, a low computational burden.

Email addresses: `crportil@unal.edu.co` (C. Portilla), `jairo.espinosa@ieee.org` (J. Espinosa), `b.deschutter@tudelft.nl` (B. De Schutter)

In general, the urban traffic models used in model-based controllers (Diakaki et al., 2000; Tettamanti et al., 2008; de Oliveira and Camponogara, 2010; Geroliminis et al., 2013; Tettamanti et al., 2014; Diakaki et al., 2002; Viti and van Zuylen, 2004; Keyvan-Ekbatani et al., 2015; Lu et al., 2017; van den Berg et al., 2003) and monitoring applications (Tiriolo et al., 2014; Adacher and Tiriolo, 2015) describe the vehicles using one generic class (average class) of vehicles, which does not allow to identify the particular dynamics of the different vehicle types. Nevertheless, multiple classes of vehicles have been included in some macroscopic models based on the generalization of the cell transmission model (Tiaprasert et al., 2017; Tuerprasert and Aswakul, 2010), in continuous models based on gas-kinetic and fluid dynamics modeling principles (Hoogendoorn and Bovy, 2000; Gashaw et al., 2018), and in cellular automata models (Meng et al., 2007; Zhao et al., 2008; Chen et al., 2013; Meng and Weng, 2011). However, these models are not adequate for real-time implementation of optimal control strategies due to their high computational burden. On the other hand, most papers about multi-class traffic modeling focus on highways (Pasquale et al., 2017; van Lint et al., 2008; Dhamaniya and Chandra, 2013; Liu et al., 2017; Wong and Wong, 2002; Logghe and Immers, 2008). Particularly, van Lint et al. (2008); Liu et al. (2017) describe the relation between vehicles for different congestion regimes on highways. On the other hand, different vehicle classes have been represented based on the Passenger Car Equivalent/Unit (PCE) concept which relates any vehicle class with a standard vehicle. Since the first definition of PCE given in the Highway Capacity Manual (TRB, 1950) that explains the effect of buses and heavy traffic with respect to other vehicles. Several studies have been carried out on adjusting the values of different classes of vehicles in PCE for different road geometries, congestion levels, and control conditions (traffic signals). The calculation methods for the PCE values mainly depend on the variables that are considered (Giuffrè et al., 2015; Shalini and Kumar, 2014), i.e., the measured or estimated variables such as flow, density, headway, queue discharge flow, speed, delay, capacity ratio, and travel time. However, taking into account that variables such as maximum acceleration, maximum speed, emissions, noise, fuel consumption, vehicle occupancy, etc. are related to the vehicle class, the equivalences given in the PCE values do not always are correct, e.g., 1 motorcycle $= 0.3 \times$ PCE could be a good approximation for traffic models but not for noise models. Since explicit models of various classes have been developed for highways, our contribution in this paper is the development of a macroscopic urban traffic model that considers different classes of vehicles separately. Based on van Lint et al. (2008); Liu et al. (2017) and on a macroscopic urban traffic model for single-class vehicles (the S model) (Lin et al., 2012), we will propose in this paper a new multi-class urban traffic model that is also suited for model-based optimization-based control applications.

This paper is organized as follows: in Section 2 the single-class S model is presented. Next, in Section 3 the new multi-class S model is proposed. Then, in Section 4 parameter estimation for the single-class and the multi-class S model is discussed. After that, in Section 5 a case study is presented that compares the performance of the multi-class and the single-class S model using a microscopic simulator (SUMO) as reference. Finally, in Section 6 conclusions and future research are presented.

2. Single-Class S Model

The S model is a macroscopic urban traffic model that was developed for single-class traffic (Lin et al., 2012). This model was based on the BLX model (Lin and Xi, 2008; Lin et al., 2009) and the Berg model (van den Berg et al., 2003), reducing the computational burden without overly decreasing the degree of accuracy of representation, which is important for real-time control applications. In order to describe the S model it is necessary take into account some definitions. As shown in Figure 1 the urban road between the intersections u and d is called link (u, d). For

every time step k two state variables are considered: $n_{u,d}(k)$ and $q_{u,d,o}(k)$, which represent the number of vehicles in the link (u,d) at time step k and the number of vehicles at time step k waiting in the queue in link (u,d) that have downstream intersection o as their next destination. For each intersection u and d the simulation time steps are counted based on the cycle time values c_u and c_d respectively, i.e., simulation time steps can be different for different intersections.

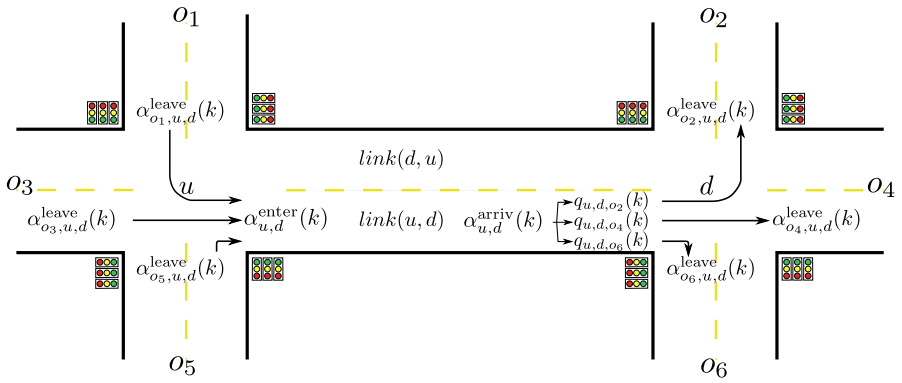

Figure 1: Two interconnected intersections in an urban traffic network.

The inflow $\alpha^{\text{enter}}_{u,d}(k)$ into link (u,d) and the outflow $\alpha^{\text{leave}}_{u,d}(k)$ from link (u,d) in the period $[k\,c_d, (k+1)\,c_d]$ are given by the sum of flows over incoming and outgoing links as follows:

$$\alpha^{\text{enter}}_{u,d}(k) = \sum_{i \in I_{u,d}} \alpha^{\text{leave}}_{i,u,d}(k), \tag{1}$$

$$\alpha^{\text{leave}}_{u,d}(k) = \sum_{o \in O_{u,d}} \alpha^{\text{leave}}_{u,d,o}(k), \tag{2}$$

where $O_{u,d}$ and $I_{u,d}$ are the set of downstream and upstream intersections from link (u,d) respectively. Moreover, the outflow towards downstream intersection o is calculated as:

$$\alpha^{\text{leave}}_{u,d,o}(k) = \min \left\{ \frac{\mu_{u,d,o}\, g_{u,d,o}(k)}{c_d}, \frac{q_{u,d,o}(k)}{c_d} + \alpha^{\text{arriv}}_{u,d}(k), \frac{\beta_{u,d,o}(k)(C_{d,o} - n_{d,o}(k))}{\sum_{i \in I_{d,o}} \beta_{i,d,o}(k) c_d} \right\}, \tag{3}$$

where $\mu_{u,d,o}$, $g_{u,d,o}(k)$, $\beta_{u,d,o}(k)$, $n_{d,o}(k)$, and $C_{d,o}$ represent the maximum outflow from link (u,d) to downstream intersection o, the green time of the traffic light for the traffic in link (u,d) going to downstream intersection o at time step k, the split ratio of vehicles going to destination o, the number of vehicles in link (d,o) at time step k, and the capacity of link (d,o) respectively. Furthermore, $\alpha^{\text{arriv}}_{u,d}(k)$ is the arriving flow at the tail of the queue, which is obtained through a variable delay $\sigma_{u,d}(k)c_d + \gamma_{u,d}(k)$ for[1] $\sigma_{u,d}(k) \leq 1$ (Jamshidnejad et al., 2018b), as follows :

$$\alpha^{\text{arriv}}_{u,d}(k) = \frac{c_d - \gamma_{u,d}(k)}{c_d} \alpha^{\text{enter}}_{u,d}(k - \sigma_{u,d}(k)) + \frac{\gamma_{u,d}(k-1)}{c_d} \alpha^{\text{enter}}_{u,d}(k - \sigma_{u,d}(k-1) - 1), \tag{4}$$

with

[1]The case $\sigma_{u,d}(k) > 1$ is more complex and is given in (Jamshidnejad et al., 2018a).

$$\sigma_{u,d}(k) = \text{floor}\left\{\frac{(C_{u,d} - q_{u,d}(k))\, l_{\text{veh}}}{N^{\text{lane}}_{u,d}\, v^{\text{free}}_{u,d}\, c_d}\right\}, \tag{5}$$

$$\gamma_{u,d}(k) = \text{rem}\left\{\frac{(C_{u,d} - q_{u,d}(k))\, l_{\text{veh}}}{N^{\text{lane}}_{u,d}\, v^{\text{free}}_{u,d}}, c_d\right\}, \tag{6}$$

where l_{veh}, $N^{\text{lane}}_{u,d}$, and $v^{\text{free}}_{u,d}$ represent the average vehicle length, the number of lanes in link (u,d), and the free-flow speed in link (u,d). Further, the remainder function is represented in (6) as "rem". The arrival flow at the tail of each queue is:

$$\alpha^{\text{arriv}}_{u,d,o}(k) = \beta_{u,d,o}(k)\, \alpha^{\text{arriv}}_{u,d}(k). \tag{7}$$

The states of the S model are defined through the following vehicle balances:

$$n_{u,d}(k+1) = n_{u,d}(k) + \left(\alpha^{\text{enter}}_{u,d}(k) - \alpha^{\text{leave}}_{u,d}(k)\right) c_d, \tag{8}$$

$$q_{u,d,o}(k+1) = q_{u,d,o}(k) + \left(\alpha^{\text{arriv}}_{u,d,o}(k) - \alpha^{\text{leave}}_{u,d,o}(k)\right) c_d, \tag{9}$$

where

$$q_{u,d}(k) = \sum_{o \in O_{u,d}} q_{u,d,o}(k). \tag{10}$$

When the cycles times c_u and c_d are not the same, it is necessary to synchronize the flow rates because the simulation steps for the intersections u (k_u) and d (k_d) are different. The leaving flow rate from intersection u can be recast into the entering flow to intersection d, by transforming the leaving flow in continuous time as:

$$\alpha^{\text{leave,cont}}_{i,u,d}(t) = \alpha^{\text{leave}}_{i,u,d}(k_u), \qquad k_u\, c_u \le t < (k_u+1)\, c_u. \tag{11}$$

Then, the average entering flow rate in time step k_d can be calculated as (see also (Jamshidnejad et al., 2018b)):

$$\alpha^{\text{enter}}_{i,u,d}(k_d) = \frac{\displaystyle\int_{k_d cd}^{(k_d+1)cd} \alpha^{\text{leave,cont}}_{i,u,d}(t)}{c_d}\, \mathrm{d}t. \tag{12}$$

The S model described by (1)–(12) represents the behavior of single-class vehicles, i.e., this model assumes vehicles with the same parameters: the average length of the vehicles and the free-flow speed. Previously, the S model has been extended in order to consider origin queues and emissions (Jamshidnejad et al., 2018b; Lin et al., 2013), but these extensions of the model also considered a single class of vehicles. However, real urban traffic networks contain different types of vehicles, so in reality there is non-homogeneous traffic. In the next section, a new extension of the S model to multi-class traffic is proposed.

3. Multi-Class S Model

In order to explain the multi-class S model, consider two interconnected intersections (u and d) as shown in Figure 1 occupied by several vehicles classes, indexed by c, where C is the number of vehicle classes. There can be several types of vehicles in an urban traffic network that can have different sizes, speeds, engines power, etc. In general, these different types of vehicles generate a non-homogeneous occupancy of the urban road, as illustrated in Figure 2.

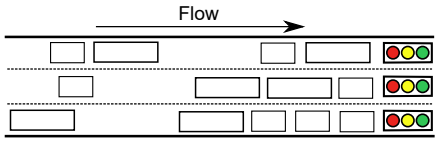

Figure 2: Non-homogeneous occupancy in an urban traffic network.

In order to describe the multi-class S model, passenger car equivalents (PCE) (HCM 1650) are introduced, which are used to represent all other classes c with respect to a representative vehicle class r. Then, based on van Lint et al. (2008) and Liu et al. (2017), the PCE ($\theta_{u,d,c}$) in link (u,d) for vehicle class c is given by:

$$\theta_{u,d,c} = \frac{s_{u,d,c} + t_{h,u,d,c} \cdot v_{u,d,c}}{s_{u,d,r} + t_{h,u,d,r} \cdot v_{u,d,r}} \tag{13}$$

where r, $s_{u,d,c}$, $t_{h,u,d,c}$, and $v_{u,d,c}$ represent the index of the reference class, the gross stopping distance of vehicle class c (i.e., the length of the vehicle including the vehicle separation with the preceding vehicle), the time headway (i.e., the minimum temporal space between two vehicles) of vehicle class c, and the speed of vehicle class c in link (u,d).

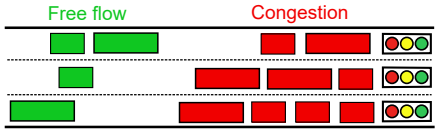

Figure 3: Free-flow and congestion regimes

In urban traffic there are mainly two regimes: free flow and congestion as illustrated in Figure 3. Vehicles are in free flow when the vehicular density in the link is small enough and the interactions between vehicles are negligible. In this regime, the vehicles are moving at the free-flow speed, which is the minimum of the maximal vehicle speed and the maximal speed allowed in the link (Kerner, 2009). On the other hand, the congestion regime is defined as "*a state of traffic in which the average speed is lower than the minimum average speed that is still possible in free flow*" (Kerner, 2009). For urban traffic networks, the congestion regime and the traffic lights generate vehicular queues. The free-flow and the congestion regimes have their own characteristics, since vehicles from different vehicle classes in free flow could have different speeds, while when vehicles are in the queue, they have the same speed regardless of which class they belong to. Taking into account (13) the PCE of the vehicles of class c in link (u,d) in the free-flow regime is given by:

$$\theta^{\text{free}}_{u,d,c} = \frac{s_{u,d,c} + t_{h,u,d,c} \cdot v^{\text{free}}_{u,d,c}}{s_{u,d,r} + t_{h,u,d,r} \cdot v^{\text{free}}_{u,d,r}}, \tag{14}$$

where $v^{\text{free}}_{u,d,c}$ is the free-flow speed of the vehicles of class c. On the other hand, the PCE of the vehicles of class c in link (u,d) in the queue is:

$$\theta^{\text{queue}}_{u,d,c} = \frac{s_{u,d,c} + t_{h,u,d,c} \cdot v^{\text{queue}}_{u,d,c}}{s_{u,d,r} + t_{h,u,d,r} \cdot v^{\text{queue}}_{u,d,r}}, \tag{15}$$

where $v^{\text{queue}}_{u,d,c}$ is the queue speed of the vehicles of class c. Assuming that $v^{\text{queue}}_{u,d,c} = v^{\text{queue}}_{u,d,r}$ and that the vehicles in the queue regime are stopped ($v^{\text{queue}}_{u,d,c} = v^{\text{queue}}_{u,d,r} \approx 0$), (15) can be rewritten as:

$$\theta^{\text{queue}}_{u,d,c} \approx \frac{s_{u,d,c}}{s_{u,d,r}}. \tag{16}$$

The total number of passenger car equivalents in the link (u,d) at time step k is:

$$n^{\text{total}}_{\text{PCE},u,d}(k) = n^{\text{free}}_{\text{PCE},u,d}(k) + n^{\text{queue}}_{\text{PCE},u,d}(k), \tag{17}$$

with

$$n^{\text{free}}_{\text{PCE},u,d}(k) = \sum_{c \in C} \theta^{\text{free}}_{u,d,c}\, n^{\text{free}}_{u,d,c}(k) \tag{18}$$

and

$$n^{\text{queue}}_{\text{PCE},u,d}(k) = \sum_{c \in C} \theta^{\text{queue}}_{u,d,c} \left(\sum_{o \in O_{u,d}} n^{\text{queue}}_{u,d,o,c}(k) \right) \tag{19}$$

where $n^{\text{free}}_{u,d,c}(k)$ and $n^{\text{queue}}_{u,d,o,c}(k)$ are the number of vehicles of class c in link (u,d) at time step k in free-flow regime and the number of vehicles of class c in the queue waiting to turn to o respectively. These two variables are considered states of the system and they are updated as follows:

$$n^{\text{free}}_{u,d,c}(k+1) = n^{\text{free}}_{u,d,c}(k) + \left(\alpha^{\text{enter}}_{u,d,c}(k) - \alpha^{\text{arriv}}_{u,d,c}(k) \right) c_d, \tag{20}$$

$$n^{\text{queue}}_{u,d,o,c}(k+1) = n^{\text{queue}}_{u,d,o,c}(k) + \left(\alpha^{\text{arriv}}_{u,d,o,c}(k) - \alpha^{\text{leave}}_{u,d,o,c}(k) \right) c_d, \tag{21}$$

where $\alpha^{\text{enter}}_{u,d,c}(k)$, $\alpha^{\text{arriv}}_{u,d,c}(k)$, $\alpha^{\text{arriv}}_{u,d,o,c}(k)$, and $\alpha^{\text{leave}}_{u,d,o,c}(k)$ are variables related with vehicles class c of link (u,d); they indicate inflow, total arriving flow at the tail of the queue, arriving flow, and outflow from the queue turning towards intersection o respectively. The inflow and outflow are described by:

$$\alpha^{\text{enter}}_{u,d,c}(k) = \sum_{i \in I_{u,d}} \alpha^{\text{leave}}_{i,u,d,c}(k), \tag{22}$$

$$\alpha^{\text{arriv}}_{u,d,c}(k) = \sum_{o \in O_{u,d}} \alpha^{\text{arriv}}_{u,d,o,c}(k), \tag{23}$$

with

$$\alpha^{\text{leave}}_{u,d,o,c}(k) = \alpha^{\text{leave}}_{\text{PCE},u,d,o}(k) \left(\frac{\theta^{\text{queue}}_{u,d,c} \left(\dfrac{n^{\text{queue}}_{u,d,o,c}(k)}{c_d} + \alpha^{\text{arriv}}_{u,d,o,c}(k) \right)}{\dfrac{n^{\text{queue}}_{\text{PCE},u,d}(k)}{c_d} + \alpha^{\text{arriv}}_{\text{PCE},u,d,o}(k)} \right), \tag{24}$$

where $\alpha^{\text{arriv}}_{\text{PCE},u,d,o}(k)$ represents the arriving PCE flow at the tail of the queue given by:

$$\alpha^{\text{arriv}}_{\text{PCE},u,d,o}(k) = \sum_{c \in C} \theta^{\text{queue}}_{u,d,c}\, \alpha^{\text{arriv}}_{u,d,o,c}(k). \tag{25}$$

The arriving flow of vehicles class c at the tail of the queue is:

$$\alpha^{\text{arriv}}_{u,d,o,c}(k) = \beta_{u,d,o,c}(k)\, \alpha^{\text{arriv}}_{u,d,c}(k), \tag{26}$$

where $\beta_{u,d,o,c}$ is the split ratio of vehicles of class c in link (u,d) going to destination o. Moreover,

$$\alpha^{\text{leave}}_{\text{PCE},u,d,o}(k) = \min \left\{ \frac{\mu_{\text{PCE},u,d,o}\, g_{u,d,o}(k)}{c_d},\ \frac{n^{\text{queue}}_{\text{PCE},u,d}(k)}{c_d} + \alpha^{\text{arriv}}_{\text{PCE},u,d,o}(k),\ \frac{\beta_{u,d,o}(k)\left(C_{\text{PCE},d,o} - n^{\text{total}}_{\text{PCE},d,o}(k)\right)}{\sum_{i \in I_{d,o}} \beta_{i,d,o}(k) c_d} \right\}. \tag{27}$$

The flow of vehicles class c that enters the link (u,d) arrives at the tail of the queue after the time $\sigma_{u,d,c}(k)c_d + \gamma_{u,d,c}(k)$ with $\sigma_{u,d}(k) \leq 1$ as follows[2] (Jamshidnejad et al., 2018b):

$$\alpha^{\text{arriv}}_{u,d,c}(k) = \frac{c_d - \gamma_{u,d,c}(k)}{c_d} \alpha^{\text{enter}}_{u,d,c}(k - \sigma_{u,d,c}(k)) + \frac{\gamma_{u,d,c}(k-1)}{c_d} \alpha^{\text{enter}}_{u,d,c}(k - \sigma_{u,d,c}(k-1) - 1), \tag{28}$$

with

$$\sigma_{u,d,c}(k) = \text{floor}\left\{ \frac{\left(C_{\text{PCE},u,d} - n^{\text{queue}}_{\text{PCE},u,d}(k)\right) l_{\text{veh},r}}{N^{\text{lane}}_{u,d}\, v^{\text{free}}_{u,d,c}\, c_d} \right\}, \tag{29}$$

$$\gamma_{u,d,c}(k) = \text{rem}\left\{ \frac{\left(C_{\text{PCE},u,d} - n^{\text{queue}}_{\text{PCE},u,d}(k)\right) l_{\text{veh},r}}{N^{\text{lane}}_{u,d}\, v^{\text{free}}_{u,d,c}}, c_d \right\}. \tag{30}$$

In order to synchronize the intersections u and d when the cycle time values c_u and c_d and thus also the simulation steps k_u and k_d are different, the leaving flow rate from intersection u is recast into the entering flow to intersection d, by transforming the leaving flow of vehicles class c in continuous time as:

$$\alpha^{\text{leave,cont}}_{i,u,d,c}(t) = \alpha^{\text{leave}}_{i,u,d,c}(k_u), \qquad k_u\, c_u \leq t < (k_u + 1)\, c_u. \tag{31}$$

Then the average entering flow rate of vehicles class c in time step k_d can be calculated as:

$$\alpha^{\text{enter}}_{i,u,d,c}(k_d) = \frac{\int_{k_d cd}^{(k_d+1)cd} \alpha^{\text{leave,cont}}_{i,u,d,c}(t)}{c_d}\, \mathrm{d}t. \tag{32}$$

The S multi-class model is presented by (14)–(32), and this model makes it possible to describe traffic flows involving several vehicle classes in an urban traffic network.

[2] A more refined model is given in (Jamshidnejad et al., 2018a).

4. Parameter estimation

The single-class S model and the multi-class S model described in Sections 2 and 3 have unknown parameters, which have to be measured or estimated. However, sometimes it is not possible to obtain a direct measure of these parameters due to the lack of sensors or due to physical limitations. As an alternative, this section presents a parameter estimation approach based on optimization, where the error is computed by comparing the estimated and measured states at each time step for the entire simulation. For this purpose, a vector $\boldsymbol{\phi}$ is defined as the parameter vector, which is different for the multi-class S model and the single-class S model. The parameter estimations of each model are presented below.

4.1. Single-class Case

Considering an urban traffic network with a set of links L and the single-class S model described in Section 2, it is possible to formulate the network model as a general non-linear model-based system as follows:

$$\hat{x}(k+1) = f(\hat{x}(k), u(k), \boldsymbol{\phi}), \tag{33}$$

where $f(\cdot)$, $\hat{x}(k)$, $u(k)$, and $\boldsymbol{\phi}$ represent the dynamic function of the estimated states, the vector of estimated states, the input vector, and the parameter vector. The estimated state vector[3] $\hat{x}(k) = (\hat{n}_{u,d}(k),\ \hat{q}_{u,d,o}(k))^{\intercal}_{(u,d)\in L,\, o\in D_{u,d}}$, contains the number of estimated vehicles and the number of estimated vehicles waiting in the queue of the set of links L, where $D_{u,d}$ is the set of downstream intersections of link (u,d). The input vector is $u(k) = (g_{u,d,o}(k), d(k), \beta_{u,d,o}(k))^{\intercal}_{(u,d)\in L,\, o\in D_{u,d}}$, where $d(k)$ is the demand for origin links of the set of links L in the period $[k\, c_d, (k+1)\, c_d]$. The parameter vector $\boldsymbol{\phi} = (\mu_{u,d,o}, C_{u,d}, l_{\text{veh}}, v^{\text{free}}_{u,d})^{\intercal}_{(u,d)\in L,\, o\in D_{u,d}}$, represents the set of unknown parameters of the set of links L. On the other hand, $x(k) = (n_{u,d}(k),\ q_{u,d,o}(k))^{\intercal}_{(u,d)\in L,\, o\in D_{u,d}}$, is the vector of measured states of vehicles in the set of links L. Further, the vector of estimated states for the set of links L of the traffic network for N_{s} simulation steps is:

$$\hat{\boldsymbol{x}} = \big(\hat{x}(k)\big)^{\intercal}_{k=1\ldots N_{\text{s}}} \tag{34}$$

where $\hat{x}(0)$ is known. In addition, the vector of measured states and the vector of inputs of the whole network are known and can be written as:

$$\boldsymbol{x} = \big(x(k)\big)^{\intercal}_{k=1\ldots N_{\text{s}}} \tag{35}$$

$$\boldsymbol{u} = \big(u(k)\big)^{\intercal}_{k=0\ldots N_{\text{s}}-1} \tag{36}$$

For the estimation, the objective function is defined by the quadratic error between the measured and estimated states as follows:

$$J(\hat{\boldsymbol{x}}, \boldsymbol{x}, \boldsymbol{u}, \boldsymbol{\phi}) = \sum_{j=1}^{N_{\text{s}}} \frac{\|\hat{x}(j) - x(j)\|^2}{\|x(j)\|^2 + 1} \tag{37}$$

Finally, the optimization problem is defined as:

[3] We use the notation $v = (a_i)_{i\in N}$ with $N = \{i_1, i_2, \ldots, i_m\}$ to define a row vector $v = [a_{i_1}\, a_{i_2} \ldots a_{i_m}]$.

$$\min_{\boldsymbol{\phi}} J(\hat{\boldsymbol{x}}, \boldsymbol{x}, \boldsymbol{u}, \boldsymbol{\phi})$$

subject to:

$$\begin{aligned} &\hat{x}(k+1) = f(\hat{x}(k), u(k), \boldsymbol{\phi}), \\ &\boldsymbol{\phi} \geq \mathbf{0}, \\ &k = 1, ..., N_{\mathrm{s}} - 1, \end{aligned} \tag{38}$$

where $\mathbf{0}$ is a vector of zeros whose dimension depends on the dimension of $\boldsymbol{\phi}$.

4.2. Multi-class Case

The parameter estimation problem for the multi-class S model described in Section 3, can be formulated like the one for the single-class S model, by using equations (34)–(38) and taking into account a general non-linear system model based can be formulated as:

$$\hat{x}(k+1) = g(\hat{x}(k), u(k), \boldsymbol{\phi}), \tag{39}$$

where $g(\cdot)$ represents the dynamic function of the estimated states, $\hat{x}(k) = (\hat{n}^{\mathrm{free}}_{u,d,c}(k),\ \hat{n}^{\mathrm{queue}}_{u,d,o,c}(k))^{\intercal}_{(u,d)\in L,\, o\in D_{u,d},\, c=1,...,C}$ is the vector of estimated states for all vehicles classes for all links, $u(k) = (g_{u,d,o}(k), d(k),\ \beta_{u,d,o,c}(k))^{\intercal}_{(u,d)\in L, o\in D_{u,d},\, c=1,...,C}$ is the input vector, and $\boldsymbol{\phi} = (s_{u,d,r}, t_{h,u,d,r},\ s_{u,d,c}, t_{h,u,d,c}, v^{\mathrm{free}}_{u,d,r}, v^{\mathrm{free}}_{u,d,c}, C_{u,d})^{\intercal}_{(u,d)\in L,\, c=1,...,C}$ is the vector of parameters for the set of links L. Further, $x(k) = (n^{\mathrm{free}}_{u,d,c}(k),\ n^{\mathrm{queue}}_{u,d,o,c}(k))^{\intercal}_{(u,d)\in L,\, o\in D_{u,d},\, c=1,...,C}$ is the vector of measured states of vehicles of class c for the set of links L.

4.3. Solution methodology

The optimization problem formulated in (38) is, in general, a non-linear and non-convex least squares problem. For this type of problems, there are usually many local minima; so the convergence to the global minimum is not guaranteed. Thus, algorithms such as multi-start sequential quadratic programming (Pardalos and Resende, 2002), simulated annealing (Eglese, 1990), pattern search (Audet and Dennis Jr, 2007), or genetic algorithms (Davis, 1991) can be used.

5. Case study and simulation results

In order to test and compare the performance of the single-class S model and the multi-class S model proposed in Sections 2 and 3, the urban traffic network depicted in Figure 4 is selected as case study. The calibration of these models is possible thanks to data collected through SUMO (Krajzewicz et al., 2012), which is a free and open source microscopic traffic simulator.
The urban traffic network shown in Figure 4 has: 8 origin-destination nodes (origins/destinations), 86 links (43 bi-directional links), and 24 internal nodes (intersections) with allowed turning directions indicated by the arrows for each lane. The case study considers cars, buses, motorcycles, and vans, which have particular characteristics, i.e., different vehicle sizes, speed, accelerations, driving conditions, etc. For this particular network the default microscopic parameters defined by SUMO were assumed. In addition, some physical and operating characteristics of the network are defined as follows:

- All links have two lanes with two directions.

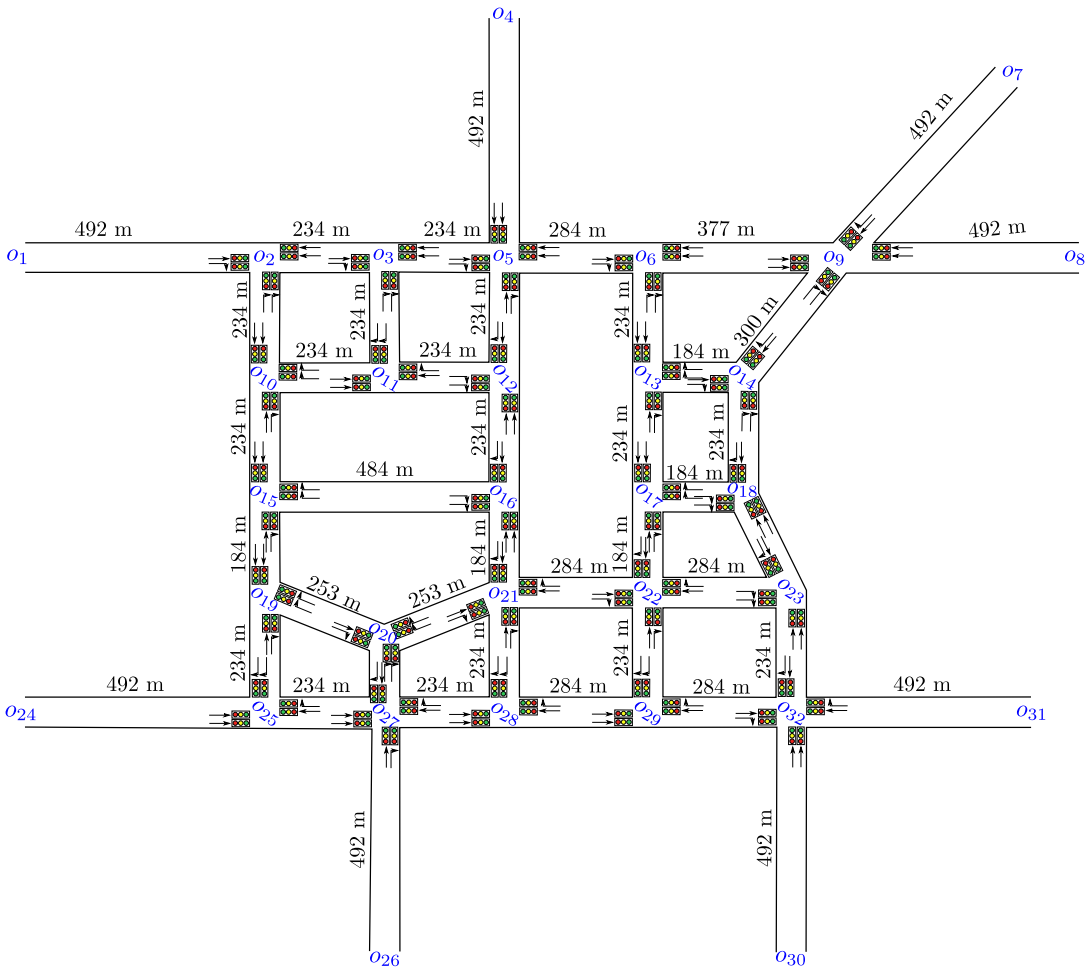

Figure 4: Urban traffic network defined for the case study

- Traffic lights have a red-amber-green configuration where the cycle time is $c_d = 90$ s, the green time is 42 s, the red time is 42 s, and the amber time is 3 s for each switch between red and green. For simplicity, the green time and the red time are fixed to the same value; then, traffic lights do not prioritize any flow direction in the intersection, keeping similar conditions for all links.
- The flow split rate on links with two allowed turning directions is 0.5 for all vehicle classes.
- The total simulation time is equal to 3 600 s.
- For simplicity, numerical identifiers for each link (link ID) are included, as presented in Table 1.

Origin nodes allow the inflow of vehicles into the network; as a result, the inflow to the origin links should be measured or estimated. The demand profiles entering to the origin links are shown in Figure 5 where demands for cars, buses, motorcycles, and vans are given in veh/h.

Table 1: Link IDs based on the layout of Figure 4.

Link ID	Link	Link ID	Link	Link ID	Link	Link ID	Link	Link ID	Link
1	(o_1, o_2)	18	(o_3, o_{11})	35	(o_{16}, o_{12})	52	(o_{19}, o_{20})	69	(o_{32}, o_{23})
2	(o_2, o_1)	19	(o_{11}, o_3)	36	(o_{13}, o_{17})	53	(o_{20}, o_{18})	70	(o_{24}, o_{25})
3	(o_2, o_3)	20	(o_5, o_{12})	37	(o_{17}, o_{13})	54	(o_{20}, o_{21})	71	(o_{25}, o_{24})
4	(o_3, o_2)	21	(o_{12}, o_5)	38	(o_{14}, o_{18})	55	(o_{21}, o_{20})	72	(o_{25}, o_{27})
5	(o_3, o_5)	22	(o_6, o_{13})	39	(o_{18}, o_{14})	56	(o_{21}, o_{22})	73	(o_{27}, o_{25})
6	(o_5, o_3)	23	(o_{13}, o_6)	40	(o_{15}, o_{16})	57	(o_{22}, o_{21})	74	(o_{27}, o_{28})
7	(o_4, o_5)	24	(o_9, o_{14})	41	(o_{16}, o_{15})	58	(o_{22}, o_{23})	75	(o_{28}, o_{27})
8	(o_5, o_4)	25	(o_{14}, o_9)	42	(o_{17}, o_{18})	59	(o_{23}, o_{22})	76	(o_{28}, o_{29})
9	(o_5, o_6)	26	(o_{10}, o_{11})	43	(o_{18}, o_{17})	60	(o_{19}, o_{25})	77	(o_{29}, o_{28})
10	(o_6, o_5)	27	(o_{11}, o_{10})	44	(o_{15}, o_{19})	61	(o_{25}, o_{19})	78	(o_{29}, o_{32})
11	(o_6, o_9)	28	(o_{11}, o_{12})	45	(o_{19}, o_{15})	62	(o_{20}, o_{27})	79	(o_{32}, o_{29})
12	(o_9, o_6)	29	(o_{12}, o_{11})	46	(o_{16}, o_{21})	63	(o_{27}, o_{20})	80	(o_{32}, o_{31})
13	(o_7, o_9)	30	(o_{13}, o_{14})	47	(o_{21}, o_{16})	64	(o_{21}, o_{28})	81	(o_{31}, o_{32})
14	(o_9, o_8)	31	(o_{14}, o_{13})	48	(o_{17}, o_{22})	65	(o_{28}, o_{21})	82	(o_{27}, o_{26})
15	(o_8, o_9)	32	(o_{10}, o_{15})	49	(o_{22}, o_{17})	66	(o_{22}, o_{29})	83	(o_{26}, o_{27})
16	(o_2, o_{10})	33	(o_{15}, o_{10})	50	(o_{18}, o_{23})	67	(o_{29}, o_{22})	84	(o_{32}, o_{30})
17	(o_{10}, o_2)	34	(o_{12}, o_{16})	51	(o_{13}, o_{18})	68	(o_{23}, o_{32})	85	(o_{30}, o_{32})

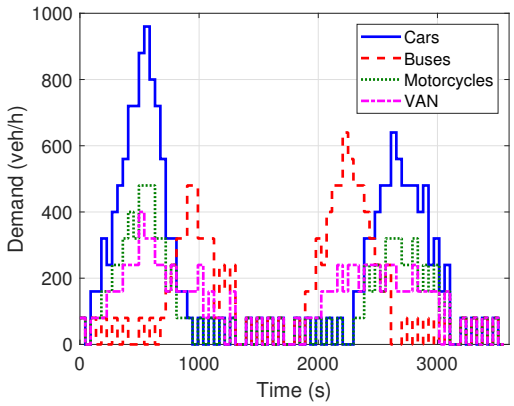

Figure 5: Vehicle demand for the origin links.

The single-class S model described by (1)–(12) and the multi-class S model described by (14)–(32) were implemented in SciTraffic (Portilla et al., 2017), which is a macroscopic simulator developed in Matlab®. For this purpose, it is necessary to code the explicit mathematical models in a particular SciTraffic module and build the urban traffic network using NETEDIT, a package included in SUMO. After that, SciTraffic can automatically create the complete macroscopic model of the network. Moreover, to transfer real-time information between SUMO and Matlab® TraCI4Matlab (Acosta et al., 2015) was used, which facilitates processes such as calibration of the models (parameter estimation), monitoring, and control of the network. To avoid getting stuck in a local minimum in the solution of the optimization problem (38), a sequential and iterative procedure of multi-start sequential quadratic programming, simulated annealing, and genetic algorithm were tested, where the initial conditions for one algorithm are given by results of the previous algorithm, e.g., the initial condition to run the simulated annealing method is provided by the result of multi-start sequential quadratic programming. The stopping criterion for the iterative process that uses the tree different algorithms is triggered when the change of

the estimation objective function value is less than 0.01% respect to the previous iteration. The performance of the multi-class model is evaluated taking into account the accuracy and computation time. For the accuracy, the absolute error described by:

$$E^{\mathrm{a}} = \sqrt{\frac{1}{N_{\mathrm{s}}} \sum_{j=1}^{N_{\mathrm{s}}} \left(x(j) - \hat{x}(j)\right)^2} \tag{40}$$

is used. Alternatively, the absolute error can be evaluated for each link separately where $E^{\mathrm{a}}_{u,d,c}$ contains the information related to link (u, d) for vehicle class c. The absolute error of the single-class S model and the multi-class S model with respect to the SUMO data for each link is presented in Figures 6 and 7. Figure 6 shows the absolute error of the number of vehicles in the traffic network for the multi-class case and the single-class case respectively, where the "x" markers denote the mean value of the error while the lines indicate the maximum and minimum error, i.e., the maximum and minimum deviation for each link. Since the multi-class S model allows to differentiate between vehicle classes, it is possible to show in Figure 6a the absolute error between this model and the SUMO data, while the single-class S model in Figure 6b shows the aggregated error for all vehicle classes.

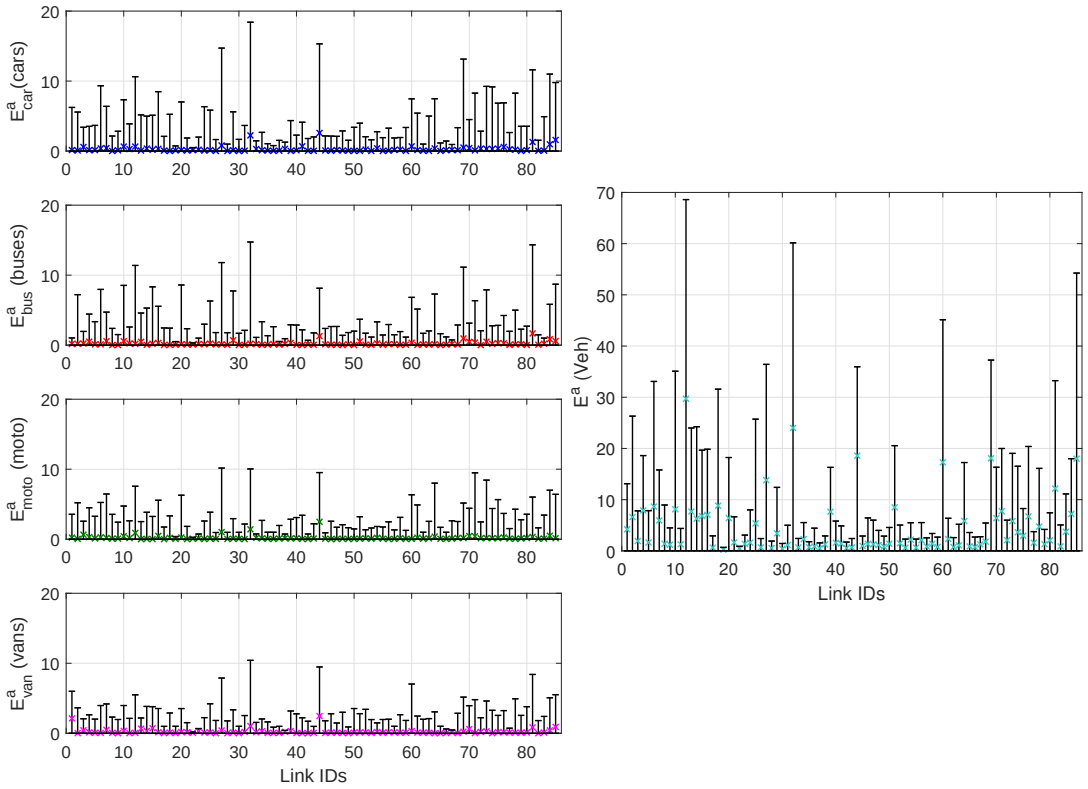

(a) Absolute error of the number of cars, buses, motorcycles, and vans for the multi-class case.

(b) Absolute error of the number of vehicles for the single-class case.

Figure 6: Absolute error of the number of vehicles in the traffic network. (a) Multi-class case, (b) Single-class case.

Likewise, Figure 7 shows the absolute error of the queue lengths for the multi-class case and the single-class case. Moreover, two representative links were selected to assess in detail the

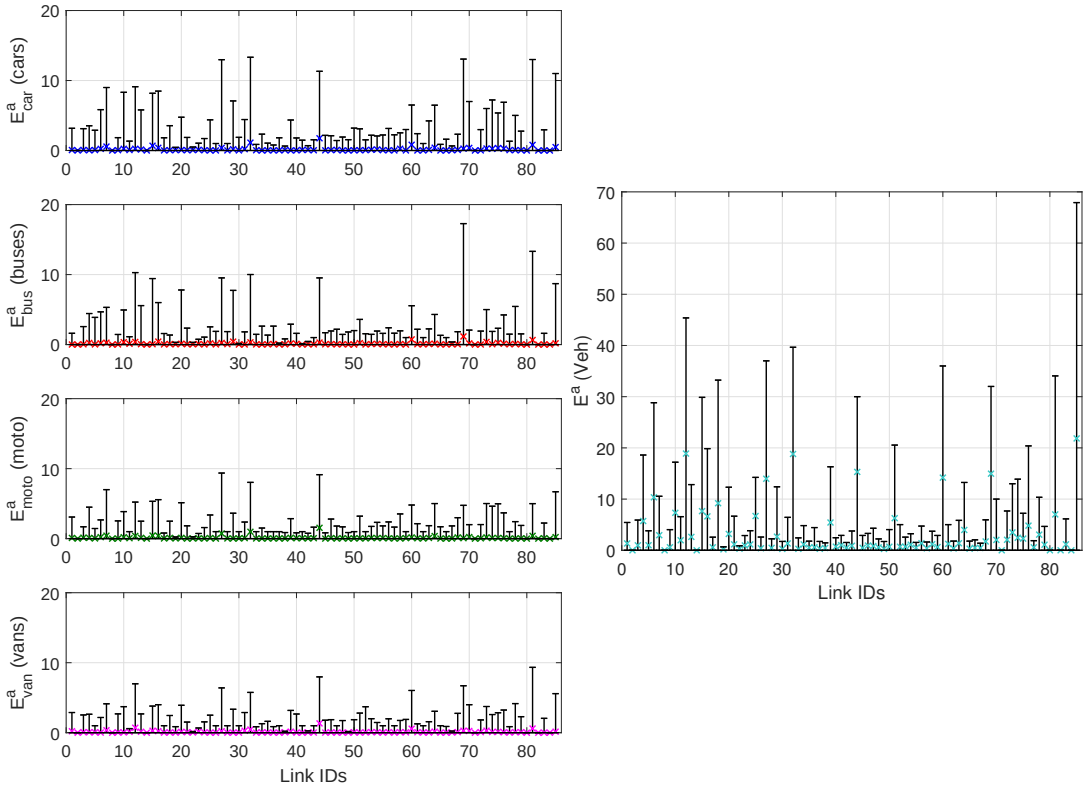

(a) Absolute error of the queue lengths of cars, buses, motorcycles, and vans for the multi-class case.

(b) Absolute error of the queue lengths of vehicles for the single-class case.

Figure 7: Absolute error of the queue of vehicles in the traffic network. (a) Multi-class case, (b) Single-class case.

behavior of the states and the errors over time. Links 1 and 32 ((o_1, o_2) and (o_{10}, o_{15})) were chosen because they are an origin link and a congested link respectively. Results for link (o_1, o_2) are presented in Figures 8 and 9. Figure 8a compares the number of cars, buses, motorcycles, and vans separately on the link (o_1, o_2) for the SUMO data and the multi-class case. Figure 8b compares the number of vehicles on the link (o_1, o_2) with the SUMO data for the single-class case. The maximal deviation for the number of vehicles between the multi-class, the single class and SUMO data are 7 cars and 13 vehicles respectively (see also Figure 6 for link 1).
In addition, Figure 9a compares the queue lengths of cars, buses, motorcycles, and vans for the SUMO data and the multi-class case and Figure 9b compares the queue of vehicles for the SUMO data and the single-class case. In the multi-class case the queue length of the multi-class case follow those of SUMO with a deviation of up to 4 cars in the worst case while for the single-class case the maximal deviation is equal to 7 vehicles, (see also Figure 7).
On the other hand, the link (o_{10}, o_{15}) is an internal link with a high occupancy; so the number of vehicles entering this link is not measured directly but calculated by means of the single-class and the multi-class S model that propagates the demand through the upstream links. The simulation results for link (o_{10}, o_{15}) are shown in Figures 10 and 11. Figure 10b shows the comparison of the number of vehicles in link (o_{10}, o_{15}) for the SUMO data and the single-class S model. From this figure, it is evident that the single-class S model does not accurately describe the demand peaks related to the increase in the number of buses (see Figure 5) because the single-class S

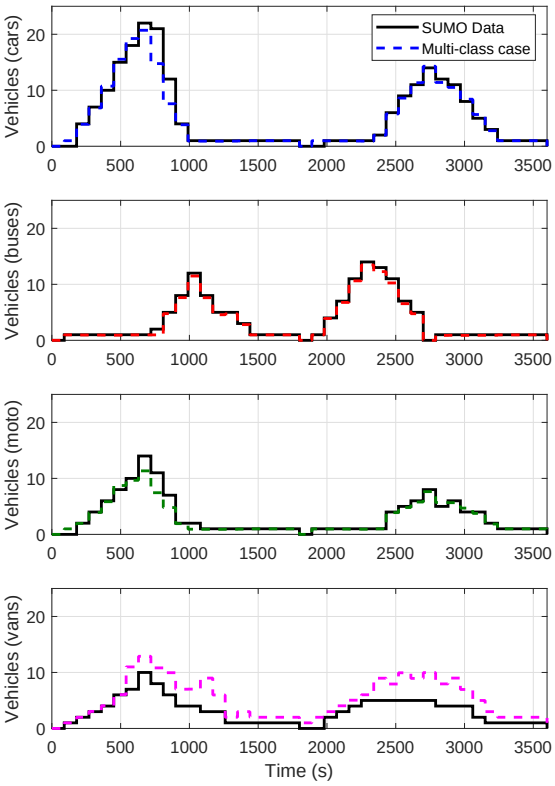

(a) Number of cars, buses, motorcycles, and vans for the multi-class case.

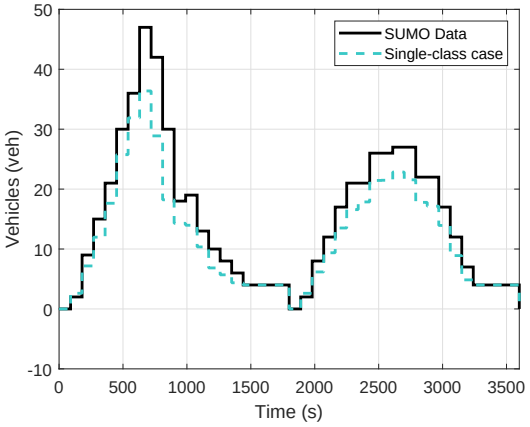

(b) Number of vehicles for the single-class case.

Figure 8: Number of vehicles of link (o_1, o_2). (a) Multi-class case, (b) Single-class case.

model includes cars, buses, motorcycles, and vans as only one class of vehicles. From Figures 10b and 6b, it is evident that the maximum error for the number of vehicles in the links is 29. Moreover, Figure 10a presents the number of cars, buses, motorcycles, and vans for the same link using the multi-class S model. Here, all vehicles are represented in a better way, since the classes are modeled separately. Also, cars, buses, motorcycles, and vans have a maximal mean absolute error of 12 cars. Figure 11b compares the queue lengths for the single-class S model and the SUMO data and supports the results presented in Figure 10b, since the peak demand of buses generates queues that are not recognized by the model. A comparison between cars, buses, motorcycles, and vans queues for the multi-class S model and the SUMO data is shown in Figure 10a. So the link (o_{10}, o_{15}) is characterized by a high error for the single-class case but a much lower error for the multi-class case.

Finally, the calculation time of SUMO, the multi-class case, and the single-class is used as a performance index related to the computational burden. The calculation time of SUMO, the multi-class case, and the single-class was obtained for different time instants as is shown in Figure 12, where the computation time for each sampling time instant (with a sample interval of 90 s) is calculated. Figure 12 shows the mean time spent by the computer running the code for the single-class S model and the multi-class S model 30 times for each sampling time instant. Each simulation includes the required processes that generate the information shown in the figures of

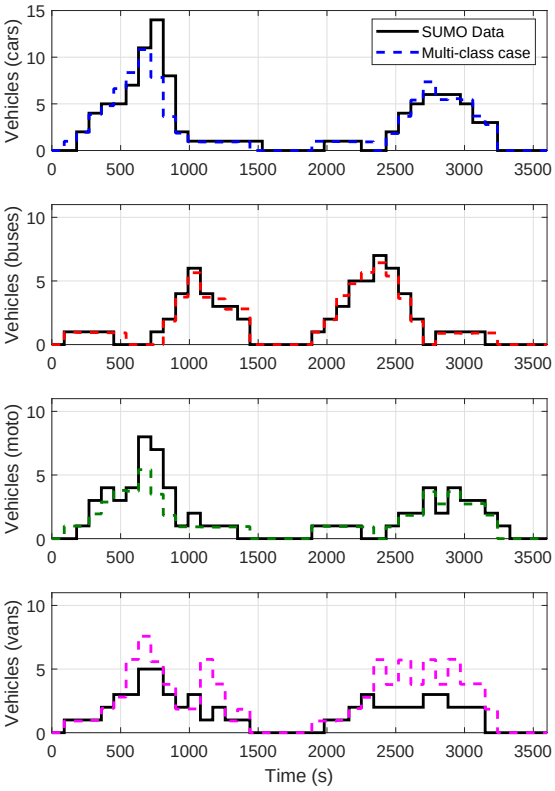

(a) Queue lengths of cars, buses, motorcycles, and vans for the multi-class case.

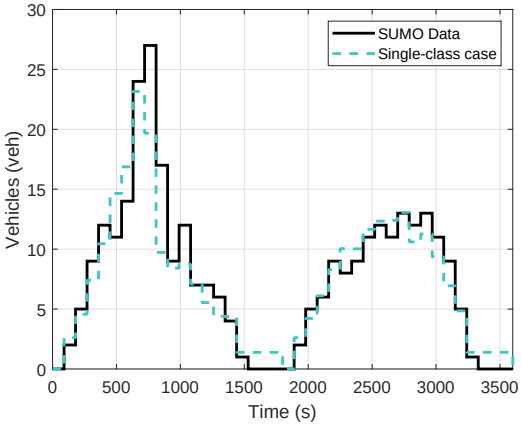

(b) Queue lengths of vehicles for the single-class case.

Figure 9: Queue lengths of link (o_1, o_2). (a) Multi-class case, (b) Single-class case.

this paper, i.e., the states must be saved and updated each sample time step. Simulations were performed on a Dell Precision Rack 7910 with a Dual Intel Xeon Processor E5-2683 v4 @ 2.1GHz (3.0GHz Turbo) and 16 cores. In Figure 12 is clear that for microscopic simulation in SUMO the CPU time increases as the number of vehicles in the network increases. On the other hand, the CPU time for the single-class and multi-class case does not depend on the number of vehicles and remains close to a mean value of 0.24 s.

Although the number of states for both models is different, i.e., the number of states of the multi-class model is C times the number of states of the single-class model, it is possible to compare the models by calculating the mean of the absolute error (40) between the states and the SUMO data for all states of each model, the results of which are shown in Table 2.

Table 2: Summary of the results

Model	Accuracy	Computational burden (1 h)	
	Error (veh)	Max (s)	Improvement (%)
Single-class case	4.9412	0.25	86.1
Multi-class case	1.1186	0.24	86.6
SUMO Data	–	1.79	–

The summarized results presented in Table 2 show that the accuracy of the multi-class case is

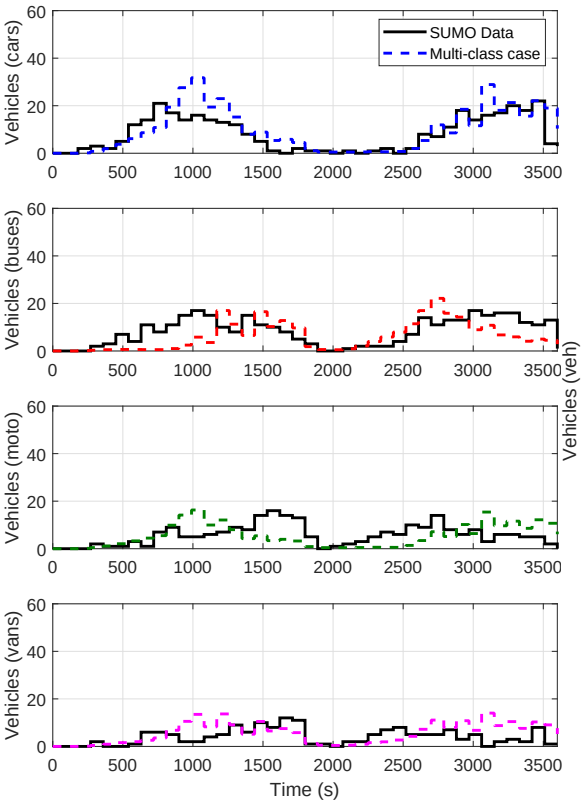

(a) Number of cars, buses, motorcycles, and vans for the multi-class case.

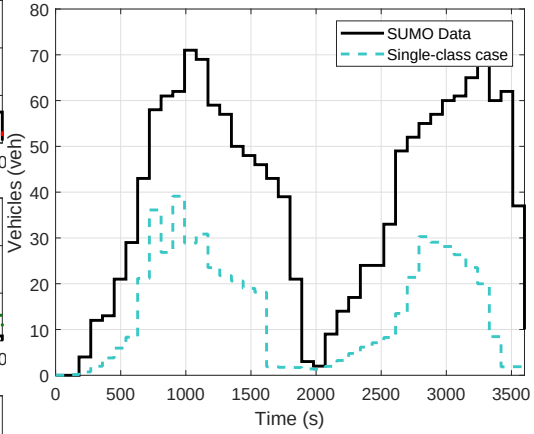

(b) Number of vehicles for the single-class case.

Figure 10: Number of vehicles of link (o_{18}, o_{14}). (a) Multi-class case, (b) Single-class case.

much higher than the single class. For the absolute error, the multi-class case improves the accuracy of the single-class case with 3.8 veh for each sampling time instant (with a sample interval of 90 s). Regarding the computational burden, the difference of the maximum CPU time between the multi-class case and the single-class case is marginal, with an improvement of at least 86.1 % with respect to the calculation time spent by SUMO.

6. Conclusions and future research

In this paper, a new multi-class urban traffic model that considers different classes of vehicles has been proposed. This model is derived from an existing single-class macroscopic model and uses the Passenger Car Equivalent (PCE) concept. Since the single-class model does not differentiate between vehicle classes, but rather assumes one generic vehicle class with average speed and length, regardless of whether the traffic is heterogeneous or not, the multi-class model is more accurate. Hence, when the vehicle composition is variable, the single-class model does not provide a good representation of traffic. The performance of the multi-class and the single-class model was compared using a case study with SUMO and it was found that the multi-class model performs much better absolute error than the single-class model. Also, the calculation time for the single-class and the multi-class model does not depend on the number of vehicles, however, the calculation time of the microsimulation in SUMO increases as the number of vehicles in

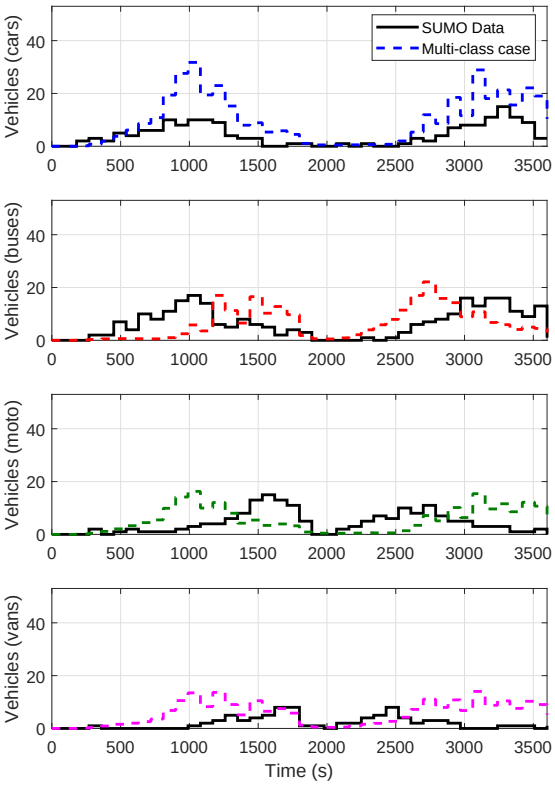

(a) Queue lengths of cars, buses, motorcycles, and vans for the multi-class case.

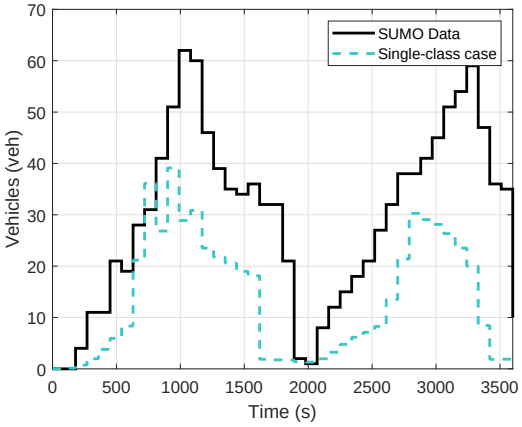

(b) Queue lengths for the single-class case.

Figure 11: Queue lengths of link (o_{18}, o_{14}). (a) Multi-class case, (b) Single-class case.

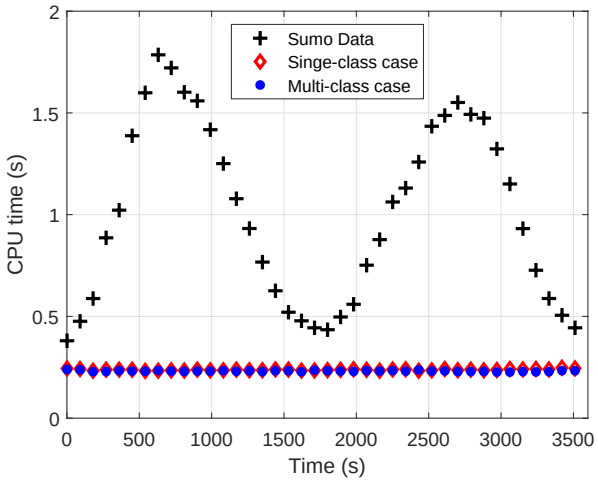

Figure 12: Comparison of the calculation time for microscopic simulation in SUMO, the single-class case, and the multi-class case.

the network increases, which limits the implementation of real-time applications on large-scale

scenarios. The main contribution of the multi-class model is that different classes of vehicles are included, increasing the representation level of the network, which is useful for control applications where it is necessary to characterize the vehicle type, i.e., control schemes with priority for certain classes of vehicles such as public transportation or monitoring of emissions discriminated by transportation mode. Indeed, some applications such as emission monitoring require the dynamic discrimination of the different classes of vehicles in the network, since using only the PCE values can cause underestimations of the emissions, i.e., the relation bus $= 2.5 \times$ PCE could be valid to traffic flow models but not for emissions models.
As a future research, the multi-class S model could be used as a prediction model in a model-based predictive controller (MPC), in order to prioritize transportation modes such as public transportation and non-motorized transportation. In addition, we will consider using data from real systems (using video analysis for vehicle classifications) for the model calibration.

7. Acknowledgments

This work was supported by COLCIENCIAS through the program "Doctorados Nacionales - Convocatoria 647" and by SAPIECIA-ENLAZAMUNDOS 2016. A special acknowledgement to COLCIENCIAS project: Reducción de emisiones vehiculares Mediante el modelado y gestión óptima de tráfico en áreas metropolitanas - caso Medellín - Area Metropolitana Valle de Aburrá, código 111874558167, CT 049-2017. Universidad Nacional de Colombia Proyecto HERMES 25374.

References

Acosta, A., Espinosa, J. E., Espinosa, J., 2015. Developing tools for building simulation scenarios for SUMO based on the SCRUM methodology. In: Proceedings of the 3rd SUMO User Conference SUMO 2015. Deutsches Zentrum für Luft - und Raumfahrt e.V., Berlin-Adlershof, pp. 23–35.

Adacher, L., Tiriolo, M., 2015. A new methodology to calibrate the congestion wave for the cell transmission model for urban traffic. In: Proceedings of the 18th IEEE International Conference on Intelligent Transportation Systems. pp. 606–611.

Audet, C., Dennis Jr, J. E., 2007. Analysis of generalized pattern searches. SIAM Journal on Optimization 13 (3), 889–903.

Chen, G., Meng, F., Fu, G., Deng, M., Li, L., 2013. A cell automation traffic flow model for mixed traffic. Procedia - Social and Behavioral Sciences 96, 1412–1419.

Davis, L. (Ed.), 1991. Handbook of Genetic Algorithms. Van Nostrand Reinhold, New York, USA.

de Oliveira, L. B., Camponogara, E., 2010. Multi-agent model predictive control of signaling split in urban traffic networks. Transportation Research Part C: Emerging Technologies 18 (1), 120–139.

Dhamaniya, A., Chandra, S., 2013. Speed prediction models for urban arterials under mixed traffic conditions. Procedia - Social and Behavioral Sciences 104, 342–351.

Diakaki, C., Papageorgiou, M., Aboudolas, K., 2002. A multivariable regulator approach to traffic-responsive network-wide signal control. Control Engineering Practice 10 (2), 183–195.

Diakaki, C., Papageorgiou, M., McLean, T., 2000. Integrated traffic-responsive urban corridor control strategy in glasgow, scotland: Application and evaluation. Transportation Research Record: Journal of the Transportation Research Board (1727), 101–111.

Eglese, R. W., 1990. Simulated annealing: A tool for operational research. European Journal of Operational Research 46 (3), 271–281.

Gashaw, S., Goatin, P., Härri, J., 2018. Modeling and analysis of mixed flow of cars and powered two wheelers. Transportation Research Part C 89, 148–167.

Geroliminis, N., Haddad, J., Ramezani, M., 2013. Optimal perimeter control for two urban regions with macroscopic fundamental diagrams: A model predictive approach. IEEE Transactions on Intelligent Transportation Systems 14 (1), 348–359.

Giuffrè, O., Granà, A., Mauro, R., Silva, A. B., Chiappone, S., 2015. Developing passenger car equivalents for freeways by microsimulation. Transportation Research Procedia 10, 93–102.

Hoogendoorn, S. P., Bovy, P. H., 2000. Continuum modeling of multiclass traffic flow. Transportation Research Part B: Methodological 34 (2), 123–146.

Jamshidnejad, A., Lin, S., Xi, Y., De Schutter, B., 2018a. Erratum to "Integrated urban traffic control for the reduction of travel delays and emissions"[IEEE Transactions on ITS, 14 (2013), 1609–1619]. IEEE Transactions on Intelligent Transportation Systems. To appear.

Jamshidnejad, A., Papamichail, I., Papageorgiou, M., De Schutter, B., 2018b. Sustainable model-predictive control in urban traffic networks: Efficient solution based on general smoothening methods. IEEE Transactions on Control Systems Technology 26 (3), 813–827.

Kerner, B. S., 2009. Introduction to Modern Traffic Flow Theory and Control: The Long Road to Three-Phase Traffic Theory. Springer, Heidelberg, Germany.

Keyvan-Ekbatani, M., Papageorgiou, M., Knoop, V. L., 2015. Controller design for gating traffic control in presence of time-delay in urban road networks. Transportation Research Part C 59, 308–322.

Krajzewicz, D., Erdmann, J., Behrisch, M., Bieker, L., 2012. Recent development and applications of SUMO - simulation of urban mobility. International Journal on Advances in Systems and Measurements 5 (3&4), 128–138.

Lin, S., De Schutter, B., Xi, Y., Hellendoorn, H., 2012. Efficient network-wide model-based predictive control for urban traffic networks. Transportation Research Part C 24, 122–140.

Lin, S., De Schutter, B., Xi, Y., Hellendoorn, H., 2013. Integrated urban traffic control for the reduction of travel delays and emissions. IEEE Transactions on Intelligent Transportation Systems 14 (4), 1609–1619.

Lin, S., De Schutter, B., Xi, Y., Hellendoorn, J., 2009. A simplified macroscopic urban traffic network model for model-based predictive control. In: Proceedings of the 12th IFAC Symposium on Transportation Systems. Redondo Beach, California, pp. 286–291.

Lin, S., Xi, Y., 2008. An efficient model for urban traffic network control. In: Proceedings of the 17th World Congress of the International Federation of Automatic Control. Seoul, Korea, pp. 14066–14071.

Liu, S., Hellendoorn, H., De Schutter, B., 2017. Model predictive control for freeway networks based on multi-class traffic flow and emission models. IEEE Transactions on Intelligent Transportation Systems 18 (2), 306–320.

Logghe, S., Immers, L., 2008. Multi-class kinematic wave theory of traffic flow. Transportation Research Part B: Methodological 42 (6), 523–541.

Lu, K., Du, P., Cao, J., Zou, Q., He, T., Huang, W., 2017. A novel traffic signal split approach based on explicit model predictive control. Mathematics and Computers in Simulation.

Meng, J. P., Dai, S. Q., Dong, L. Y., Zhang, J. F., 2007. Cellular automaton model for mixed traffic flow with motorcycles. Physica A: Statistical Mechanics and its Applications 380, 470–480.

Meng, Q., Weng, J., 2011. An improved cellular automata model for heterogeneous work zone traffic. Transportation Research Part C 19 (6), 1263–1275.

Pardalos, P. M., Resende, M. G. C. (Eds.), 2002. Handbook of Applied Optimization. Oxford University Press, Oxford, UK.

Pasquale, C., Sacone, S., Siri, S., De Schutter, B., 2017. A multi-class model-based control scheme for reducing congestion and emissions in freeway networks by combining ramp metering and route guidance. Transportation Research Part C 80, 384–408.

Portilla, C., Acosta, A., Espinosa, J., Espinosa, J., 2017. SciTraffic: A macroscopic simulator for estimation and control of urban traffic. In: Proceedings of the SUMO User Conference 2017. Berlin-Adlershof, pp. 80–88.

Shalini, K., Kumar, B., 2014. Estimation of the passenger car equivalent: A review. International Journal of Emerging Technology and Advanced Engineering 4 (6), 97–102.

Tettamanti, T., Luspay, T., Kulcsár, B., Péni, T., Varga, I., 2014. Robust control for urban road traffic networks. IEEE Transactions on Intelligent Transportation Systems 15 (1), 385–398.

Tettamanti, T., Varga, I., Kulcsar, B., Bokor, J., 2008. Model predictive control in urban traffic network management. In: Proceedings of the 16th Mediterranean Conference on Control and Automation. pp. 1538–1543.

Tiaprasert, K., Zhang, Y., Aswakul, C., Jiao, J., Ye, X., 2017. Closed-form multiclass cell transmission model enhanced with overtaking, lane-changing, and first-in first-out properties. Transportation Research Part C 85, 86–110.

Tiriolo, M., Adacher, L., Cipriani, E., 2014. An urban traffic flow model to capture complex flow interactions among lane groups for signalized intersections. Procedia - Social and Behavioral Sciences 111, 839–848.

TRB, 1950. Highway Capacity Manual. Transportation Research Board, Washington, D.C.

Tuerprasert, K., Aswakul, C., 2010. Multiclass cell transmission model for heterogeneous mobility in general topology of road network. Journal of Intelligent Transportation Systems 14 (2), 68–82.

van den Berg, M., Hegyi, A., De Schutter, B., Hellendoorn, J., 2003. A macroscopic traffic flow model for integrated control of freeway and urban traffic networks. In: Proceedings of the 42nd IEEE Conference on Decision and Control. Maui, Hawaii, pp. 2774–2779.

van Lint, J., Hoogendoorn, S., Schreuder, M., 2008. Fastlane: New multiclass first-order traffic flow model. Transportation Research Record: Journal of the Transportation Research Board 2088, 177–187.

Viti, F., van Zuylen, H., 2004. Modeling queues at signalized intersections. Transportation Research Record: Journal of the Transportation Research Board 1883, 68–77.

Wong, G., Wong, S., 2002. A multi-class traffic flow model – an extension of LWR model with heterogeneous drivers. Transportation Research Part A: Policy and Practice 36 (9), 827–841.

Zhao, X. M., Jia, B., Gao, Z. Y., Jiang, R., 2008. Congestions and spatiotemporal patterns in a cellular automaton model for mixed traffic flow. In: Proceedings of the Fourth International Conference on Natural Computation. Los Alamitos, USA, pp. 425–429.